Supporting Information

Kennett et al. 10.1073/pnas.0906374106

SI Methods

Incremental sediment samples from the Arlington Canyon geological section (AC-003) were dried and weighed. Sediments were then disaggregated, and "elongate" and spherical carbon particles were extracted via flotation and hand picked using a light microscope. Carbon elongates (≈10–15) and spherules from each stratum were grouped and crushed to a powder in 3.7-mL glass vials and mixed with 4–5 drops of 100% alcohol (ETOH) to suspend the carbonaceous powder. This admixture was pipeted to a 200-mesh copper TEM grid and dried. A representative random sample of grid cells (≈5%) was scanned for diamonds with JEOL 1200EX II, JEOL 1210, or FEI Titan transmission electron microscopes. A TEM was used to identify and image single and clustered crystals, and the diamond polymorphs were identified via selected area electron diffraction. Diamonds ranged in size between 2–1,500 nm, and crystallographic work was restricted to clusters of small crystals or larger single crystals capable of producing diffraction patterns. Multiple measurements were taken across large diamonds to determine purity. Low electron beam voltages (60–80 kV) were used because n-diamonds and lonsdaleite are metastable and vaporize at high temperatures. N-diamond concentrations inside carbon spherules were calculated using the volume of bulk sediment, the average diameter of the carbon spheres in each level, the percentage containing n-diamonds, the percentage by volume of n-diamonds in carbon spherules, and the average size of n-diamonds. Standard techniques were used for scanning electron microscope imaging. EDS and EELS analysis demonstrated that the nanoparticles identified as diamonds via selected area diffraction contain only carbon.

Soot samples were extracted and analyzed using standard procedures described by Wolbach (1, 2). Sediment samples were dried, weighed, and then demineralized using alternating 9 M HCl and 10 M HF/1 M HCl treatments to dissolve carbonates and silicates. The resultant carbonaceous residue was oxidized for 600 h with 0.2 M $Na_2Cr_2O_7$/2.0 M H_2SO_4 to selectively destroy organic carbon. The elemental carbon residue was dried, weighed, and examined on the SEM, where any soot particles present were identified by their characteristic aciniform ("bunch of grapes") morphology and quantified using image particle size analysis.

1. Wolbach WS, Lewis RS, Anders E (1985) Cretaceous extinctions: Evidence for wildfires and search for meteoritic impact. *Science* 230:167–170.
2. Wolbach WS (1990) Carbon across the Cretaceous-Tertiary boundary. PhD thesis, (Univ of Chicago, Chicago).
3. Haynes CV, Jr (2008) Younger Dryas "black mats" and the Rancholabrean termination in North America. *Proc Natl Acad Sci USA* 105:6520–6525..
4. Kennett DJ, et al. (2008) Wildfire and abrupt ecosystem disruption on California's Northern Channel Islands at the Ållerød-Younger Dryas boundary (13.0–12.9 ka). *Quaternary Sci Rev* 27:2528–2543.
5. Oleinik GS, Valter AA, Erjomenko GK (2003) The structure of high pressure lonsdaleite diamond grains from the impactites of the Belilovka (Zapadnaja) astrobleme (Ukraine). *34th Annual Lunar and Planetary Science Conference, March 17-21, 2003* (League City, Texas), 1561 (abstr).

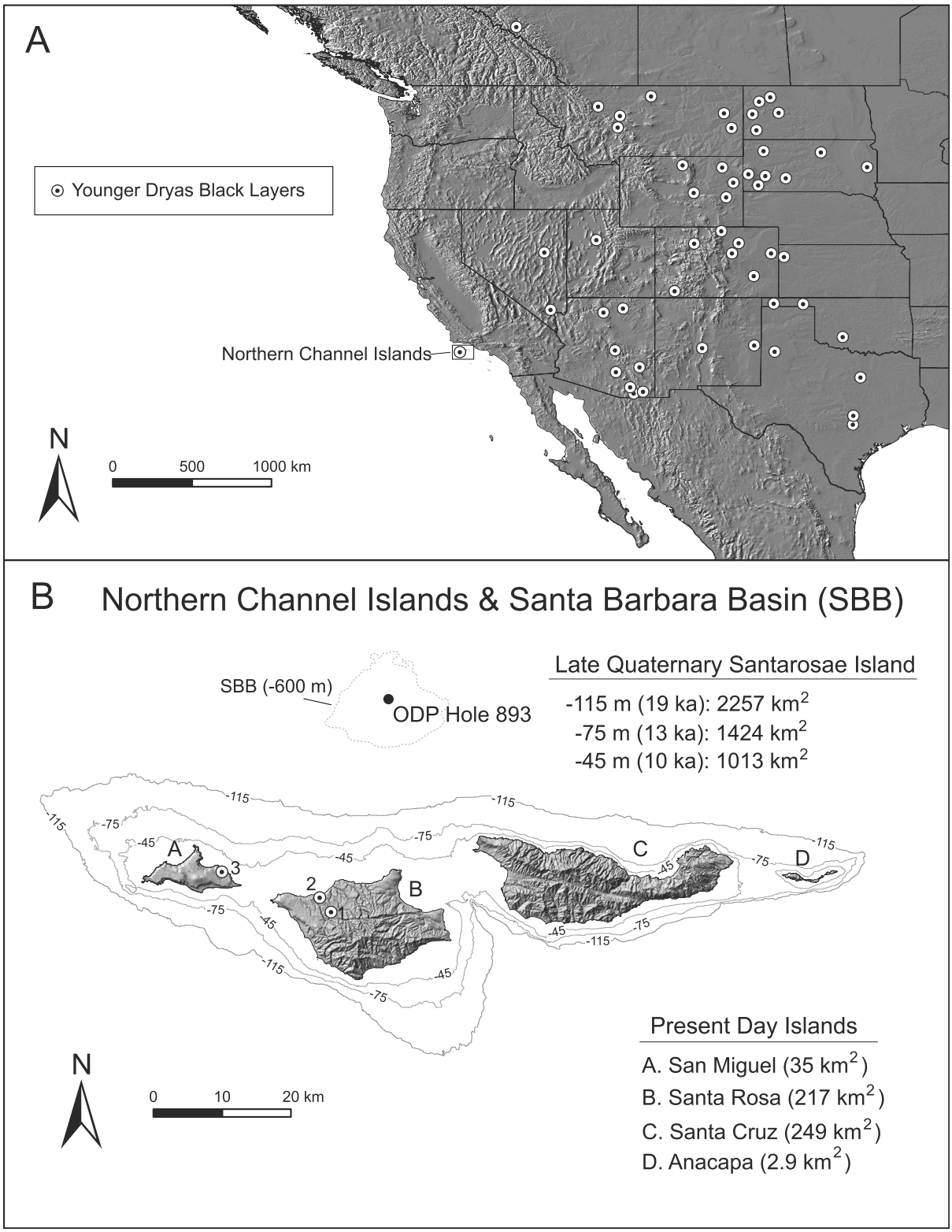

Fig. S1. Maps of western North America and Northern Channel Islands showing localities discussed in the text. (*A*) The distribution of black sedimentary layers in western North America is based on Haynes (3). (*B*) See Kennett et al. (4) for details about the bathymetry surrounding the Northern Channel Islands. Localities identified on the Northern Channel Islands are indicated by numbers: 1, Arlington Canyon (AC-003); 2, Arlington Springs Human locality (CA-SRI-173); 3, Daisy Cave. (Figure layout by Jacob Bartruff.)

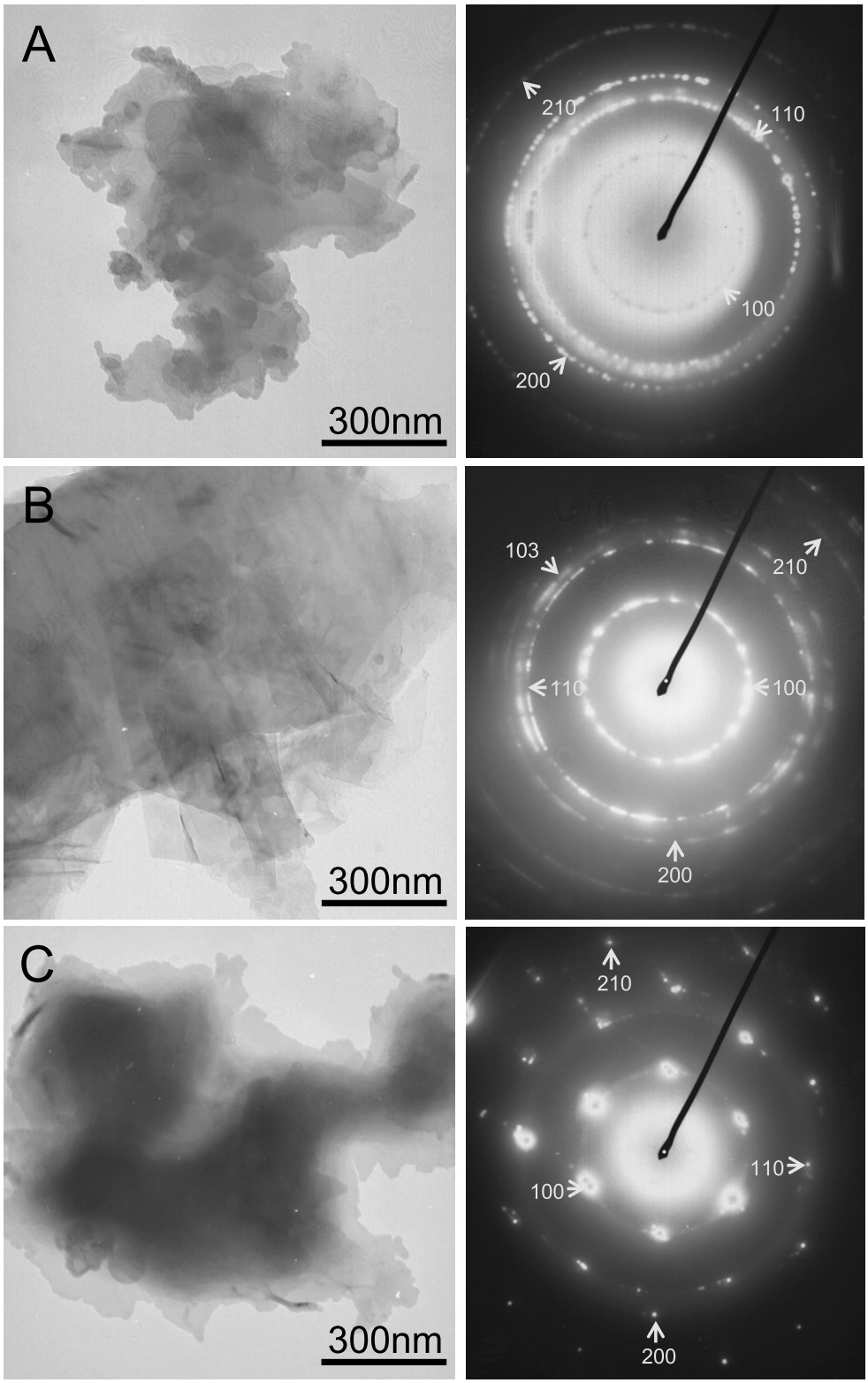

Fig. S2. Additional TEM photomicrographs (*Left*) and diffraction patterns (*Right*) of hexagonal diamond polymorphs in the YDB (12.95 ± 0.05 ka) sedimentary layer in Arlington Canyon (AC-003). (*A*) Cluster of lonsdaleite crystals and associated diffraction pattern from 4.64 and 4.69 m (AC#347); (*B*) cluster of lonsdaleite crystals and associated diffraction pattern from 4.59–4.64 m (AC#348); (*C*) close-up of single lonsdaleite crystal and associated diffraction pattern from 4.59–4.64 m (AC#348)—note lamellae. See Fig. 1 for stratigraphic position of samples.

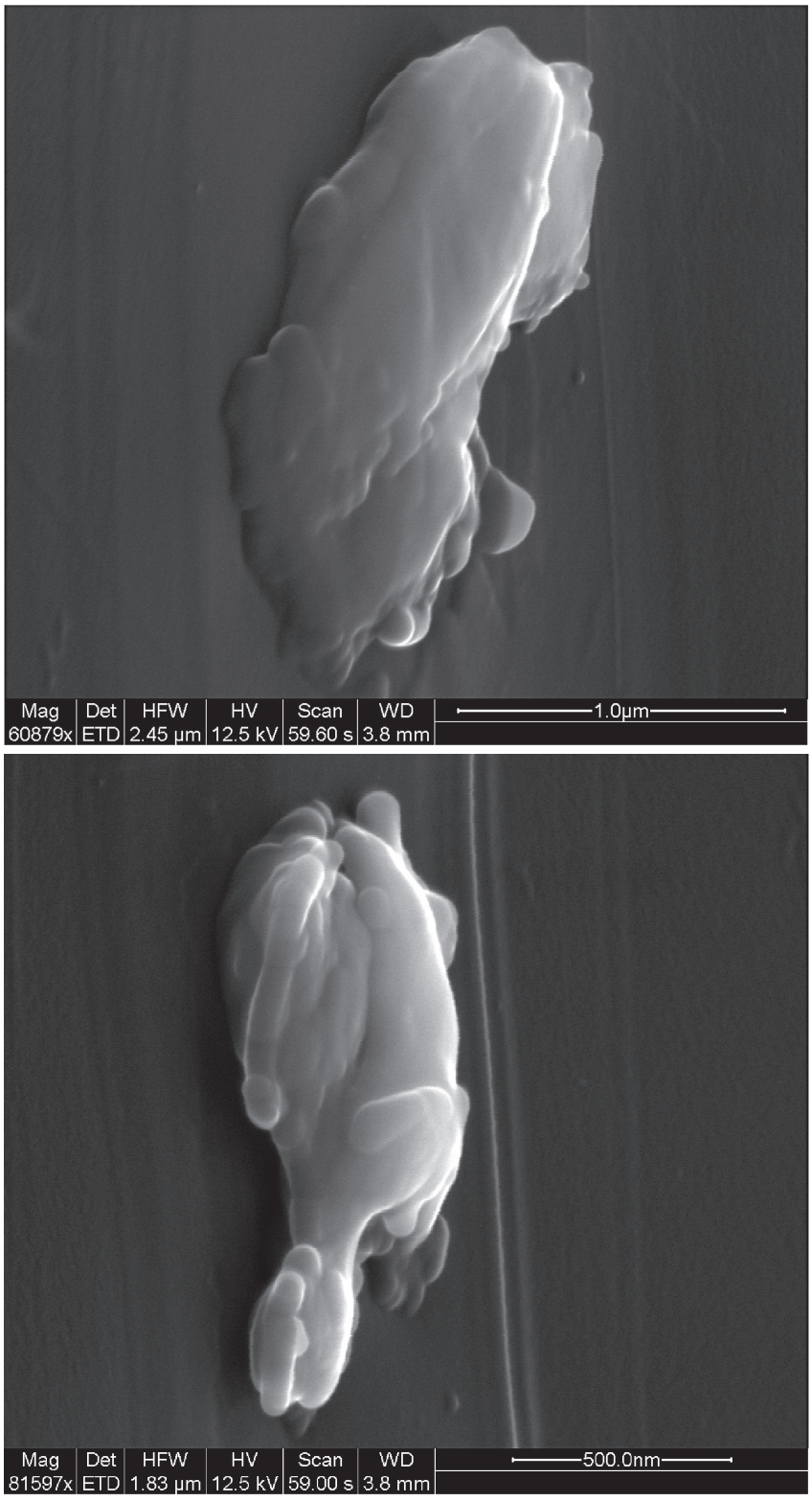

Fig. S3. Oblique SEM images of lonsdaleite crystal clusters shown in Fig. 2.

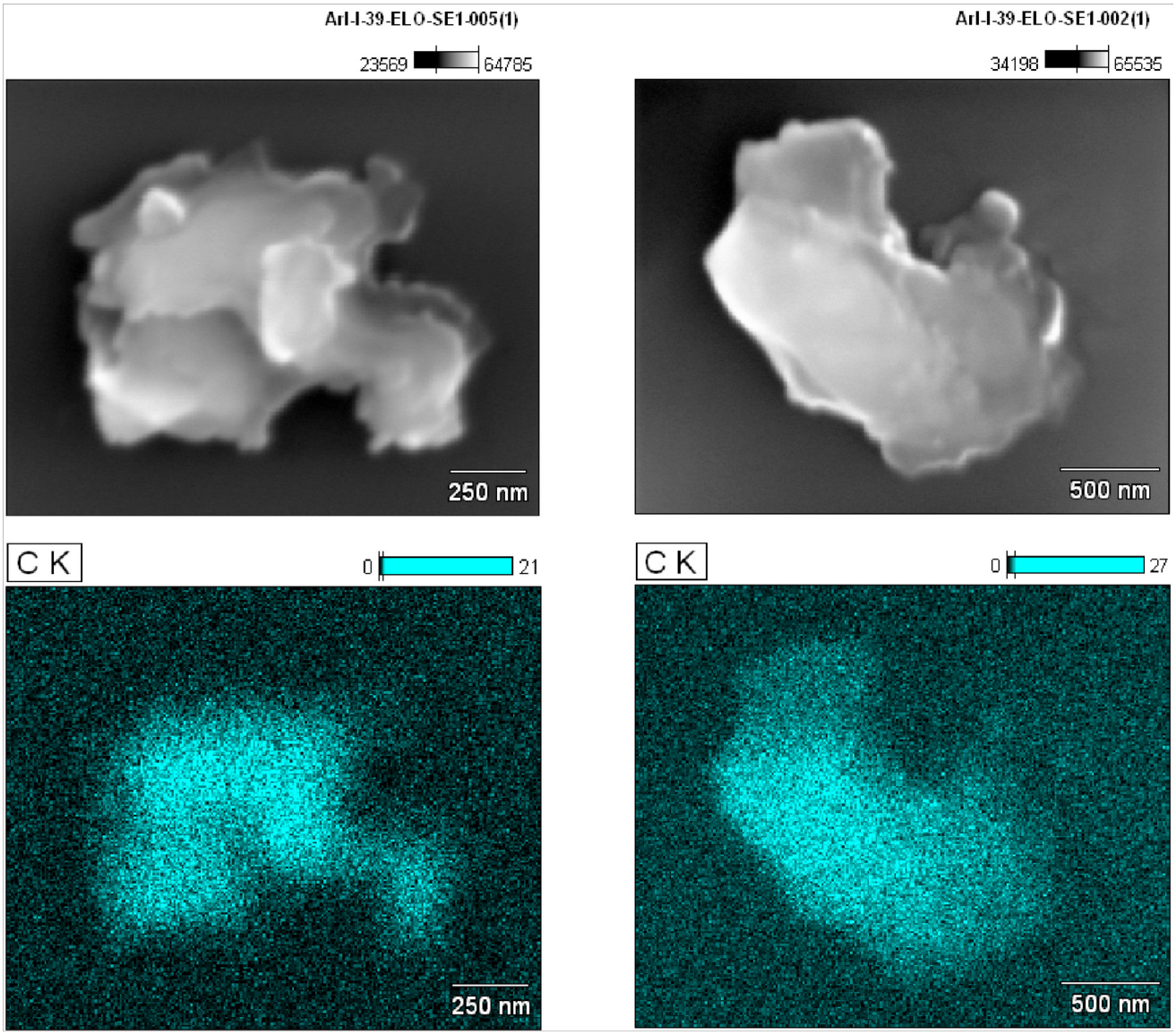

Fig. S4. Image map of EDS spectra of lonsdaleite crystal clusters shown in Fig. 2 that demonstrates dominant carbon composition.

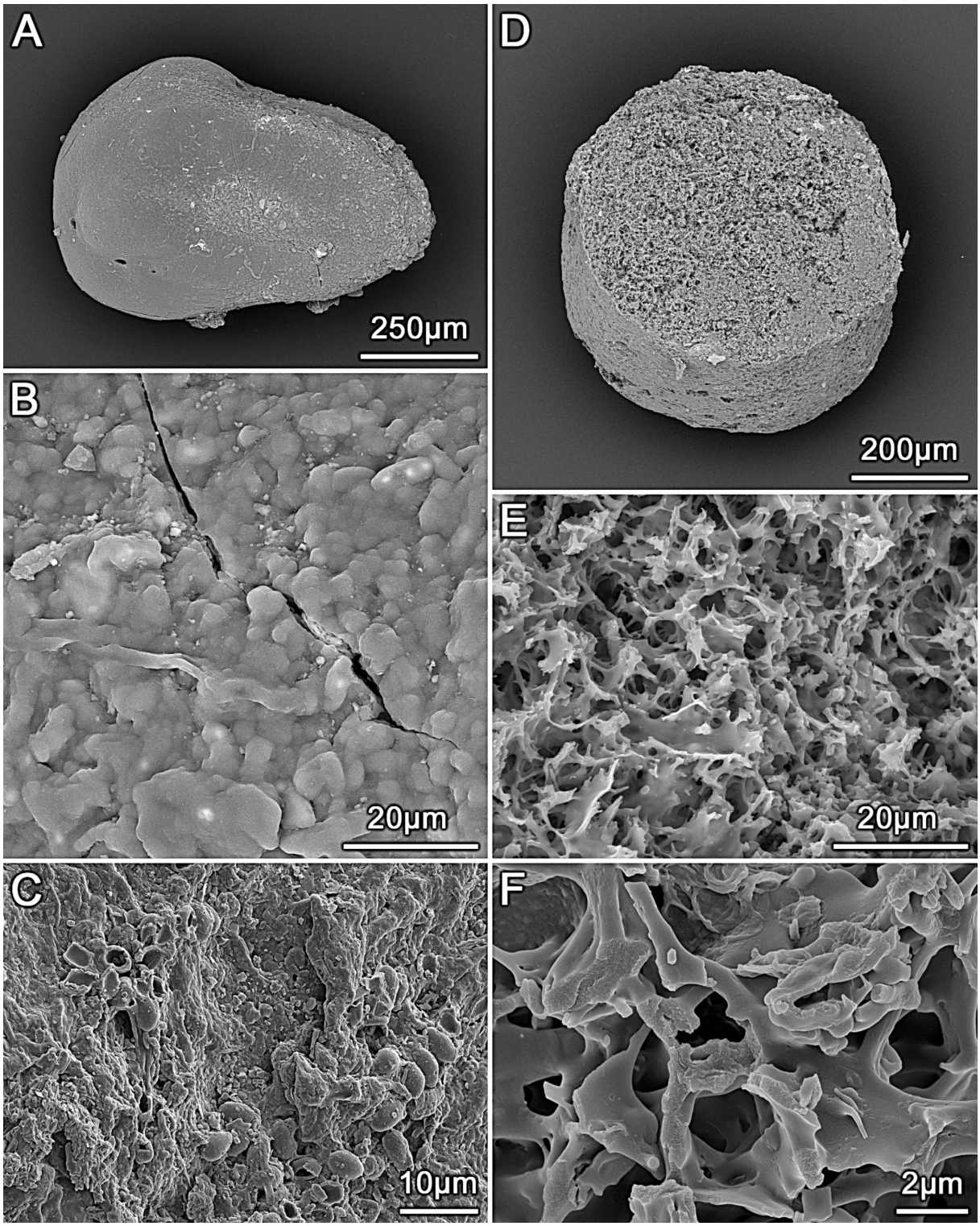

Fig. S5. SEM images of carbon elongates from YDB layer in Arlington Canyon Section, Santa Rosa Island, California (basal black layer). (*A*) Large, subangular carbon elongate showing smooth and glassy surface. (*B*) Surface microstructure at about midpoint (to the left) of elongate in *A* showing relatively smooth relief (botryoidal texture) due to melting. (*C*) Surface microstructure of edge (to the right) of carbon elongate shown in *A* showing roughness (with hollow bean-like structures of unknown origin). (*D*) Bisected, carbon elongate with relatively rounded exterior showing interior structure of complex, nonreticulate walls and voids. (*E*) Irregular, complex, nonreticulate interior of carbon elongate shown in *D* that illustrates well-vitrified and brittle thin walls of amorphous carbon separating voids. (*F*) Higher magnification image of complex, irregular interior of same elongate as in *D* and *E*. Walls are made of massive, highly vitreous, amorphous carbon.

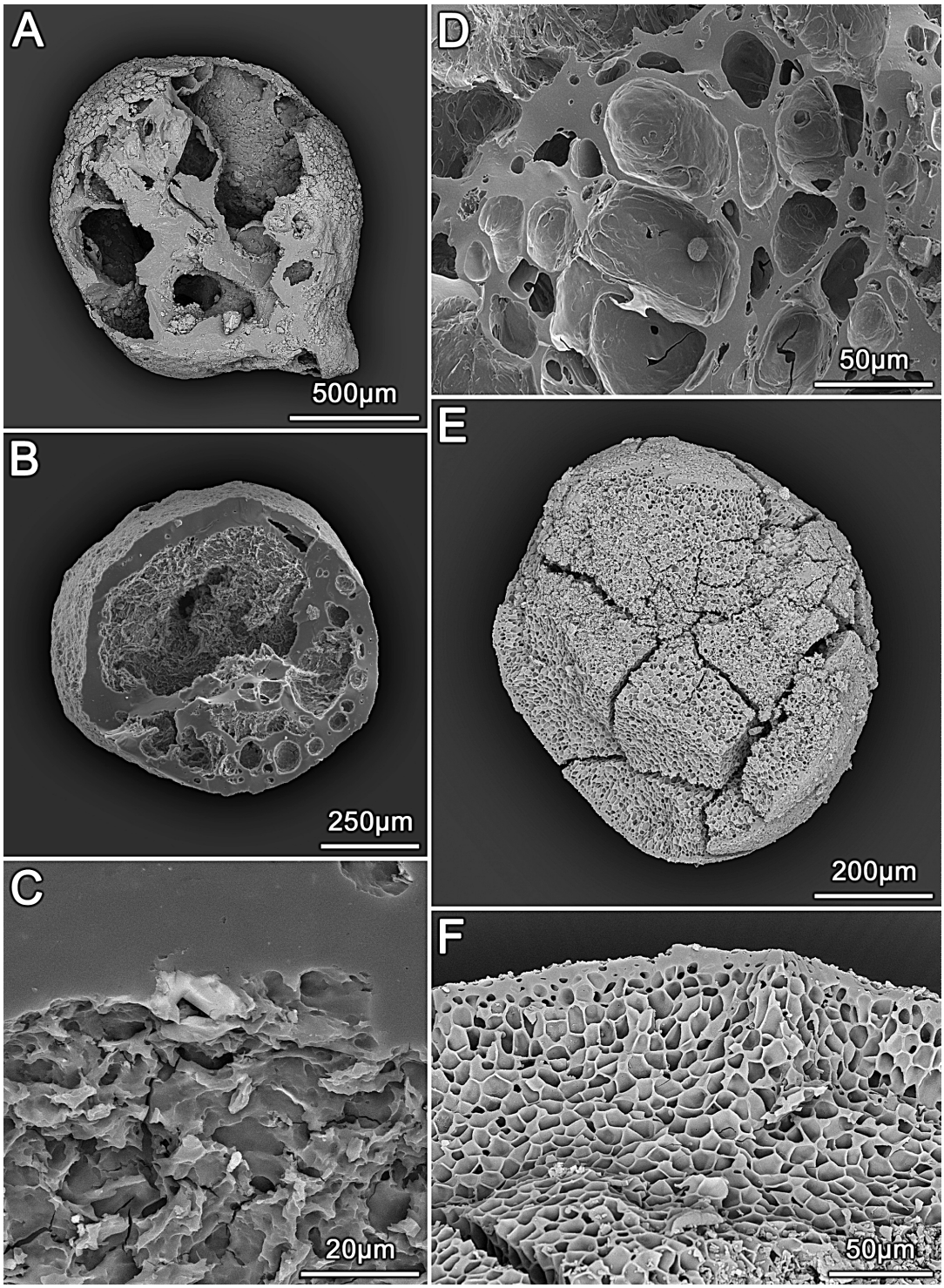

Fig. S6. SEM images of carbon elongates and carbon spherules from YDB layer (basal black layer), Arlington Canyon section, Santa Rosa Island, California. (*A*) Carbon elongate, strongly vitrified walls throughout (surface and interior) containing large voids. (*B*) Bisected carbon elongate, strongly vitrified structure throughout, with thick, massive rind containing voids and hollow center with complex, irregular structure. (*C*) More magnified image of carbon elongate shown in *B* illustrating massive, complex outer crust and irregular, complex interior walls and voids. (*D*) Interior vesicles of strongly vitrified carbon elongate. (*E*) Bisected carbon spherule showing typical internal reticulate (honeycomb) structure and thin, nonreticulate crust. (*F*) Close-up of carbon spherule interior shown in *E* with well-organized reticulate (honeycomb) structure and thin, nonreticulate crust. Carbon spherules differ from carbon elongates by having well-organized, reticulate, rather than irregular, complex interiors.

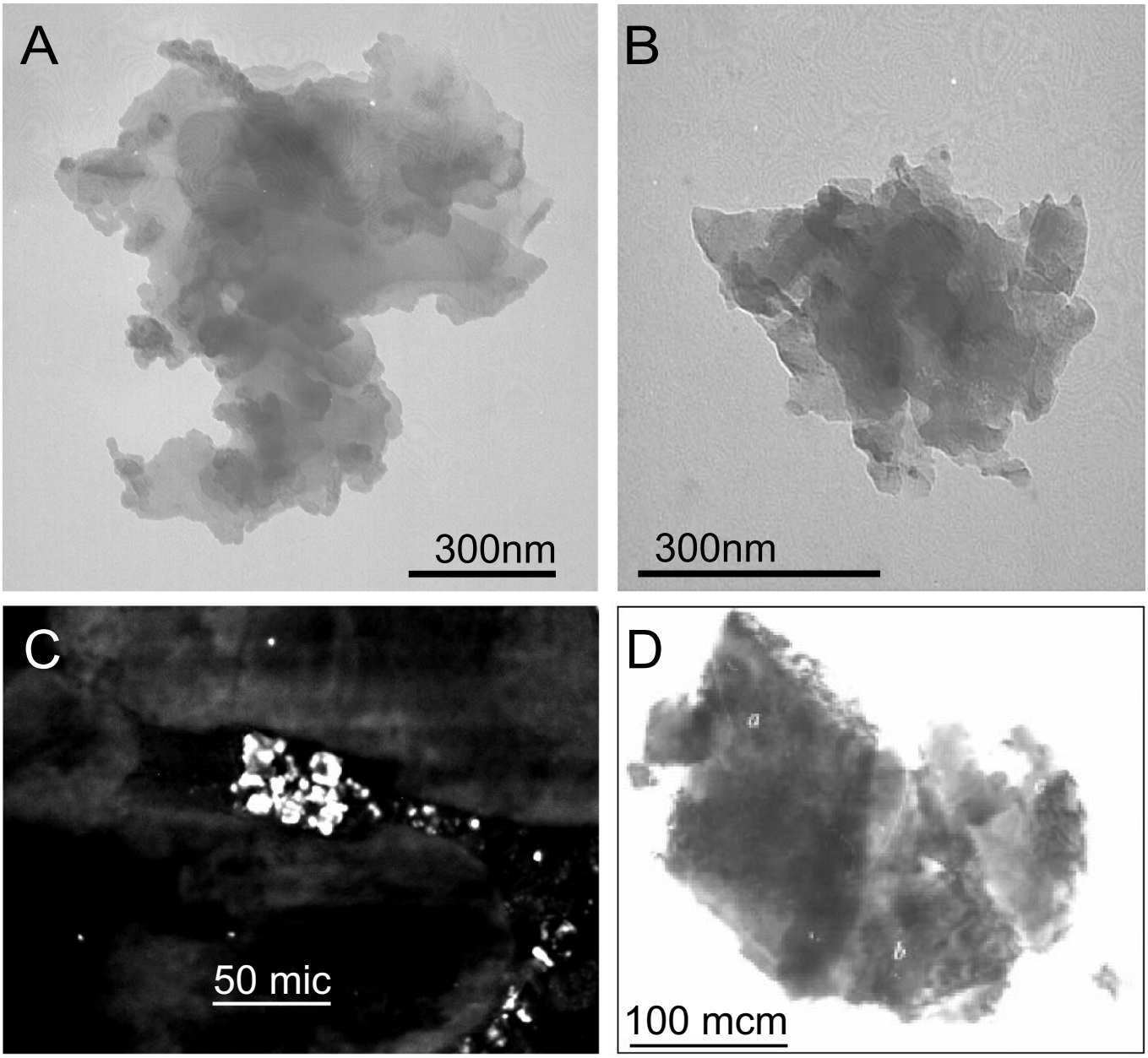

Fig. S7. Images of hexagonal diamond clusters. Diamond clusters were obtained from: (*A*) ≈12.95 ± 0.05 ka deposits in Arlington Canyon (TEM); (*B*) African Ureilite NWA 2971 (TEM); (*C*) African Ureilite NWA 2971 (cathodoluminescence, SEM); (*D*) Belilovka impact crater (5). The SEM image (*C*) shows in situ hexagonal diamonds set in thermally decomposed graphite (dark).

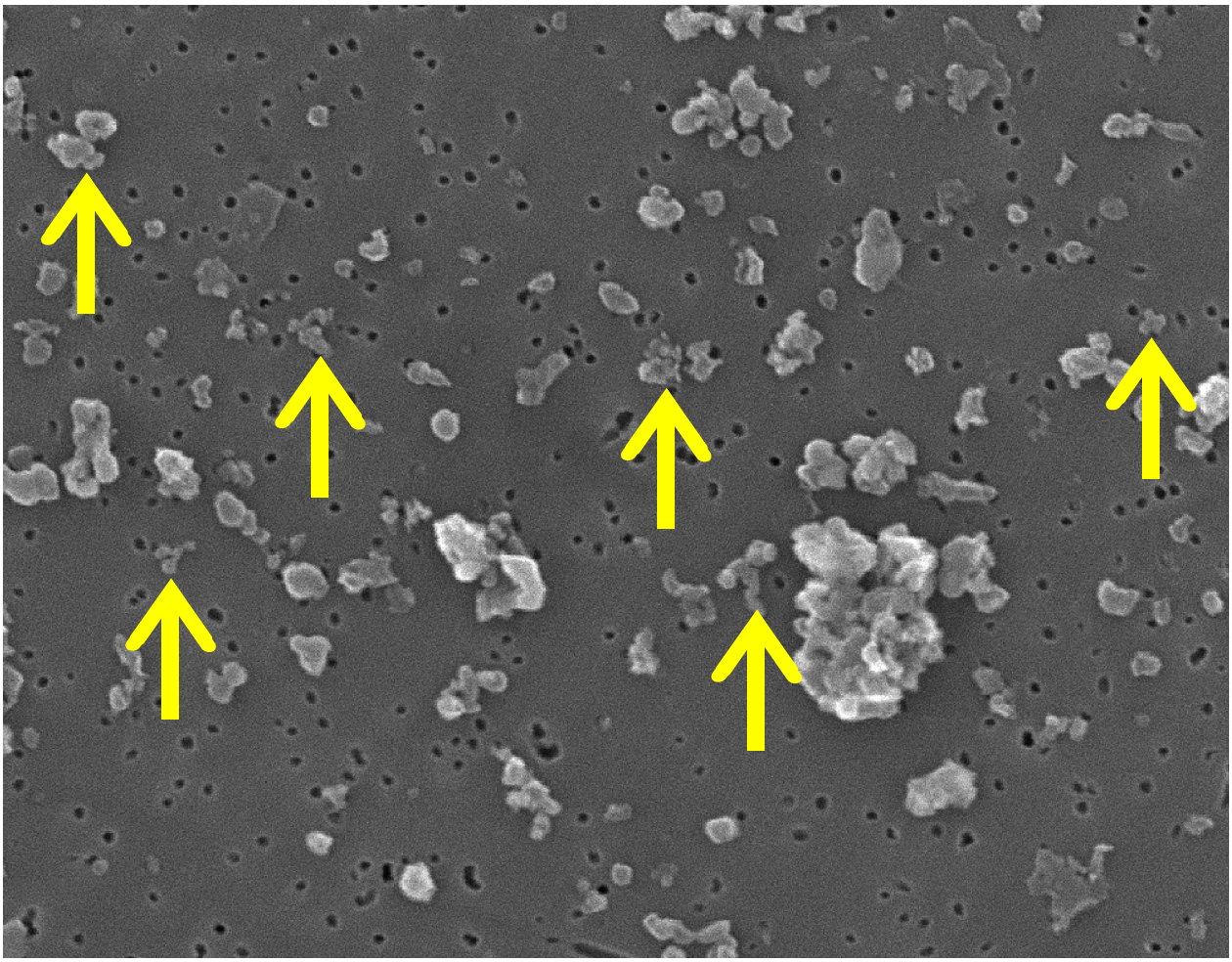

Fig. S8. SEM micrograph of grape-clustered soot (examples marked by yellow arrows) from Arlington Canyon. Highest concentrations were identified in level AC 343 (2,500 ± 250 ppm), with trace amounts found in AC344 (13 ± 1 ppm). High abundances of soot are consistent with impact-triggered fires and sudden burial favoring preservation.

Table S1. Quantitative distribution of organic carbon, other carbon forms (e.g., wood and herbaceous charcoal, various carbon particles, soot), and diamonds in sediment samples from Arlington Canyon (AC-003)

								Diamonds						
			Charcoal		Carbon			N-Diamonds			Cubic	Hexagonal	Soot	
Sample no.	cmbs	% Organic C	Wood no./cm^3	Herbaceous, %	Spherules, no./kg	Elongate, no./kg	Glasslike, g/kg	In CS, ppb*	In Elongate, ppb*	Total, ppb	No. detected	No. detected	ppm	±
AC318	95–99†	1.870	115	7.83	0	192	0.000	0	0	0				
AC319	115–120†	2.080	2	0.00	0	0	0.000	0	0	0				
AC320	122–125	2.044	0	0.00	0	0	0.000	0	0	0				
AC321	145–148	2.601	0	0.00	0	0	0.000	0	0	0				
AC322	166–169	3.870	0	0.00	0	0	0.000	0	0	0				
AC323	179–183	2.175	18	0.00	0	0	0.000	0	0	0				
AC324	195–198	1.991	413	8.72	0	23	0.001	0	0	0				
AC325	215–217	3.459	131	0.00	0	112	0.001	0	0	0				
AC326	226–229	1.920	31	0.00	0	30	0.001	0	0	0				
AC327	238–241	2.437	2	0.00	0	0	0.000	0	0	0				
AC328	245–248	1.416	22	0.00	0	31	0.001	0	0	0				
AC329	267–270	1.688	76	1.32	0	66	0.000	0	0	0				
AC330	297–300	2.838	65	0.00	0	0	0.001	0	0	0				
AC331	340–343	1.769	5	0.00	0	0	0.000	0	0	0				
AC332	383–386	1.648	13	0.00	0	18	0.000	0	18	18	1000			
AC333	392–396	3.583	261	0.00	0	767	0.001	0	1342	1342		1		
AC334	403–406	2.959	430	0.23	0	173	0.001	0	363	363				
AC335	413–416	2.785	0	0.00	0	0	0.000	0	0	0				
AC348	459–464	3.025	51	0.00	8	42	0.001	0	35	35		40		
AC347	464–469	3.577	58	0.00	31	81	0.001	0	26	26		24		
AC346	469–475	3.075	132	0.00	68	193	0.001	0	0	0				
AC345	475–480	3.929	102	0.00	13	113	0.001	0	0	0				
AC344	480–485	3.720	148	0.00	190	264	0.001	53	0	53			13	1
AC343	485–491	4.472	849	0.24	85	249	0.001	12	0	12			2500	250
AC342	491–493	8.719	435	6.90	38	0	0.000	0	0	0			0	0
AC341	493–498	4.069	258	1.55	166	373	0.001	73	0	73			0	0
AC340	498–503	4.310	268	0.37	274	714	0.001	0	855	855			0	0

Diamond polymorphs include n-diamonds in carbon spherules and elongates and hexagonal and cubic found only in association with elongates.
*Embedded in carbonaceous matrix.
†Profile 2.